



Degradation of mefenamic acid using magnetic multi-walled carbon nanotube as a novel particle electrode in a three-dimensional electro-Fenton process

Mohammad Reza Zare^a, Nezamaddin Mengelizadeh^{a,*}, Hamidreza Pourzamani^{b,c}, Yaghoob Hajizadeh^{b,c}, Heidar Mohammadi^d, Morteza Khodadadi Saloot^e

^aResearch Center of Health, Safety and Environment, Department of Environmental Health Engineering, Evaz School of Health, Larestan University of Medical Sciences, Larestan, Iran, Tel. +98-939-231-2472; emails: Nezam_m2008@yahoo.com (N. Mengelizadeh), zaremohammad1363@yahoo.com (M.R. Zare)

^bEnvironment Research Center, Research Institute for Primordial Prevention of Non-communicable disease, Isfahan University of Medical Sciences, Isfahan, Iran

^cDepartment of Environmental Health Engineering, School of Health, Isfahan University of Medical Sciences, Isfahan, Iran, emails: pourzamani@hlth.mui.ac.ir (H. Pourzamani), y_hajizadeh@hlth.mui.ac.ir (Y. Hajizadeh)

^dDepartment of Occupational Health Engineering, School of Health, Larestan University of Medical Sciences, Larestan, Iran, email: H.mohammadi@Larums.ac.ir (H. Mohammadi)

^eDepartment of Environmental Engineering, Faculty of Natural Resources and Environment, Science and Research Branch, Islamic Azad University, Tehran, Iran, email: morteza.khodadadi.s@srbiau.ac.ir

Received 25 June 2019; Accepted 1 January 2020

ABSTRACT

Electrocatalytic degradation of mefenamic acid (MFA) by magnetic multi-walled carbon nanotubes (MMWCNTs), as a novel particle electrode, was studied in a three-dimensional electro-Fenton (3DEF) reactor. The physicochemical properties of MMWCNTs were determined by field emission scanning electron microscopy, transmission electron microscopy, Fourier transform infrared spectroscopy and X-ray diffraction (XRD) techniques. The effect of variables and their interaction during the oxidative degradation of MFA was evaluated using response surface methodology (RSM) based on 5 levels of 5 factorial central composite design (CCD). The RSM results showed a suitable quadratic polynomial model for explaining the relationship between electrocatalytic activity and operational parameters ($R^2 = 99.6$). The optimization results indicated that maximum MFA degradation efficiency (98.36%) could be obtained at pH of 6.2, MFA concentration of 6.19 mg/L, the current density of 19.94 mA/cm², MMWCNTs dosage of 69.13 mg/L, and reaction time of 82.95 min. Comparative experiments showed further production of hydroxyl radical ($\cdot\text{OH}$) and higher electrocatalytic activity of the 3DEF system. The MMWCNTs particle electrode showed excellent stability and reusability for MFA oxidation. 3,4-dimethyl benzaldehyde and 3-methylbut-2-enoic acid were identified as MFA degradation intermediates using dispersive liquid-liquid microextraction combined with gas chromatography-mass spectrometry (GC-MS).

Keywords: Mefenamic acid; MMWCNTs; Three-dimensional electro-Fenton; Response surface methodology; Degradation pathway

1. Introduction

In recent years, the pharmaceuticals and the personal care products (PPCPs) as a class of micro-pollutants have

attracted the attention of most countries worldwide because of their environmental and health effects [1,2]. These emerging contaminants in concentrations of ng/L to $\mu\text{g/L}$ have been identified in the effluent of the pharmaceutical industries, municipal and hospital wastewater, surface and ground waters [2]. PPCPs include different classes of chemicals

* Corresponding author.

such as antibiotics, antiepileptics, and non-steroidal anti-inflammatory drugs (NSAIDs), among which the non-steroidal drugs are the most commonly used compounds for the treatment of mild to moderate pain, fever and rheumatic disorders [3,4]. NSAIDs, due to the characteristics such as bio-concentration factor of 1–1.31, $\log K_{ow}$ of 3–4.5 and pKa of 3.5–4.5 have the ability of resistance in an aqueous environment [5]. Mefenamic acid (MFA, 2-[2,3-dimethylphenyl]aminobenzoic acid) is used as a strong NSAID in the treatment of osteoporosis, sports injuries and other musculoskeletal disorders [6]. This compound is a pollutant derived from diphenylamine that is classified as a priority pollutant on the European Union list. Most of the previous studies reported that MFA is not effectively removed by conventional sewage treatment plants and produces toxicity in case of release into the environment [4,7,8]. Hence, the need for an effective and advanced technology for the removal of MFA from wastewater and, subsequently, from the environment, is essential.

Conventional methods used for removing the NSAIDs from aqueous solutions include adsorption onto activated carbon, membrane and chemical oxidation processes. According to previous studies, these processes have major disadvantages, such as the use of high energy and chemicals, the need for disposing of wastes, low efficiency of activated carbon in the removal of polar organic compounds, and the transmission of contamination from one phase to another [9]. In contrast, advanced oxidation processes (AOPs) have demonstrated more potential for treating a wide range of emerging pollutants such as pharmaceutical compounds. The AOPs, with in-situ production of reactive oxygen species (ROs) with the low selectivity such as H_2O_2 , $O_2^{\cdot-}$, O_3 and $\cdot OH$, lead to degrading pollutants into H_2O , CO_2 , inorganic ions, or acids [10]. AOPs based on the production of ROs include ultrasonic processes, UV radiation, Fenton, photo-Fenton, photo-catalytic and electrochemical oxidation processes. Among them, the electrochemical oxidation has recently attracted more attention due to its environmental compatibility and easy operation [11–13]. In this process, the degradation of organic pollutants occurs through direct and indirect oxidation. In the direct oxidation, pollutants can be oxidized by direct charge transfer due to adsorbed radical hydroxyl ($M(HO^{\cdot})$) and oxygen in oxide lattice ($MO_x^{\cdot+}$). In the indirect oxidation, the organic compounds can be degraded through in-situ production of reactive species such as H_2O_2 , ClO and O_3 [14,15]. Electro-Fenton (EF) is an indirect oxidation process from which H_2O_2 can be produced by two-electron reduction (Eq. (1)) and then converted to $\cdot OH$ (Eq. (2)) through the reaction with Fe^{2+} ions [16]. This method has significant advantages compared with the chemical Fenton process, such as high degradation rate, continuous production of H_2O_2 at the cathode surface, continuous regeneration of Fe^{2+} ions on the cathode surface, and low sludge production [17]. However, in spite of its high oxidation and mineralization ability, the EF process has disadvantages such as the need to operate at acidic pH, the loss of soluble iron, and the need for a filtration process to separate it [16].



To overcome the disadvantages of conventional EF systems and to improve the efficiency of pollutant treatment, most researchers proposed a 3DEF system containing particles between anode and cathode electrodes [18]. In this process, the particles, in a suitable density, are polarized to the charged microelectrodes, which not only shortens the distance between the electrodes and the pollutant but also leads to increased conductivity, mass transfer and also provides more active sites for catalytic and adsorption reactions [18–20]. In addition, the presence of various iron oxide species, especially Fe_3O_4 , on the supporting material reduces the loss of iron through the transfer of electrons between ferrous and ferric ions [21]. Regarding these cases, in 3D processes, the type of particle electrode material is one of the important parameters determining the efficiency, improving the current transfer and forming a suitable composite with metals. For this purpose, different materials such as nickel foam [21], kaolin [18], carbon [22], MWCNTs [20], manganese slag [19], bentonite [23], etc. have been used in recent years. Among the particle electrodes, MWCNTs have unique properties such as high surface area, good chemical and mechanical stability, high electrocatalytic effect, and resistance to corrosion [24,25]. In addition, the excellent electrical conductivity of MWCNTs can lead to the generation of reactive species through the non-radical pathway and to facilitate the catalytic processes involved in electron transfer [26,27]. Recently, according to the above-mentioned properties, MWCNTs have been used in various studies as supporting materials, adsorbents and catalysts. El-Khouly and Fathy [28] investigated the activity of Fe_2O_3 and $Ag_2O-Fe_2O_3$ supported on MWCNTs as Fenton catalysts for degradation of maxilon red dye. They found that MWCNTs with the high surface area leads to adsorb the molecules of contaminants and to improve their degradation rates. Xu et al. [24] reported that MWCNTs can increase the catalytic activity of Fe_3O_4 by adsorbing them. Chen et al. [29] found that carbon nanotubes (CNTs) with suitable functional groups had high activity in the activation of peroxy monosulfate to degrade orange acid 7. Shen et al. [30] reported that CNTs, by absorbing the dissolved oxygen, lead to its electrochemical reduction to H_2O_2 . In addition, Yu et al. [31] studied the loading of CNTs on the graphite felt cathode for more degradation of diclofenac and reported that CNTs, through the more production of H_2O_2 , lead to increase in the removal of total organic carbon than the unloaded electrode.

Due to the unique features of MWCNTs and the risks of MFA in the aquatic ecosystem, few studies on the 3DEF oxidation of MFA with magnetic MWCNTs have been performed. Hence, the purpose of this study was to synthesize MMWCNTs as a new particle electrode for the degradation of MFA in the 3DEF reactor. In addition, the optimization of operating parameters such as initial pH, current density, electrolysis time, MMWCNTs dosage and MFA concentration was performed by RSM based on CCD. Different electro-oxidation systems were used to examine the advantage of MMWCNTs as a 3DEF particle electrode. The stability and recyclability of the particle were evaluated through the electrocatalytic reaction cycle. The byproducts of MFA reaction for the first time were detected by DLLME/GC-MS, and the possible pathway of its degradation was proposed.

2. Materials and methods

2.1. Chemicals and electrodes

Ferric chloride ($\text{FeCl}_3 \cdot \text{H}_2\text{O}$), ammonium (NH_3), sodium sulfate (Na_2SO_4), chloroform (CHCl_3) and acetone ($\text{C}_3\text{H}_6\text{O}$) were provided from the Merck Company, German. Mefenamic acid (purity > 98%) as the target contaminant was purchased from Sigma-Aldrich (USA). Multi-walled CNT (purity $\geq 95\%$) was provided as a supporting material and particle electrode from US research nanomaterials (Houston, USA). N-Methyl-N-(trimethylsilyl) trifluoroacetamide (MSTFA) was purchased as a derivatizing agent from Sigma-Aldrich (USA). The MFA stock solution was prepared by dissolving the appropriate amount of powder in deionized water. A Ti/TiO₂-RuO₂ anode electrode was synthesized according to the method described in our previous study [25]. The synthesis of MMWCNTs particle electrode was also performed according to the method reported in Iranpour et al. [20] study.

2.2. Experimental procedure

Electro-oxidation experiments were carried out in a 500 mL batch electrochemical Plexiglas reactor. Ti/TiO₂-RuO₂ (9 cm × 5 cm × 1 mm) and graphite felt (10 cm × 5 cm × 1 mm) were used as anode and cathode electrodes, respectively and the space between them was filled with MMWCNTs. The initial pH of the solution containing MFA was adjusted by 0.1 mol/L H₂SO₄ or NaOH. DC power supply was used to provide the current between the anode and cathode electrode as well as to polarize the particle electrode. In order to ensure the continuous production of H₂O₂ by electrochemical reduction of the oxygen on the cathode, the aeration of the reactor was carried out by an air compressor (Helia, Taiwan). In order to increase electron transfer and disperse the particles, in all experiments, the solution was gently mixed by the magnetic bar. At the end of the reaction, the samples were withdrawn from the reactor and then filtered by 0.45 μm filter paper for further analysis.

2.3. Experimental design

The response surface methodology coupled with central composite design (RSM-CCD) was used to investigate the effect of operating parameters (initial pH, current density, electrolysis time, MMWCNTs dosage and MFA concentration), and the interaction between them on the MFA degradation efficiency. The purposes of this method are to optimize and check the interference at unrecognizable points and to estimate the probable response in these points. The CCD

method with orthogonal experiment design was performed for five variables at five levels (2, 1, 0, -1 and -2). In order to prevent pure error and, subsequently, lack of fit in the tests' results, eight replicates were added to the center points. Table 1 shows values, levels of variables, and their corresponding codes. The quadratic polynomial model displayed in Eq. (3) was used to determine the relationship between the response and the variables.

$$Y = \beta_0 + \sum_{j=1}^k \beta_j X_j + \sum_{j=1}^k \beta_{jj} X_j^2 + \sum_{i < j} \beta_{ij} X_i X_j + e_i \quad (3)$$

where Y is the response, X_i and X_j are the encoded independent variables, β_0 is the constant coefficient, β_j , β_{jj} and β_{ij} are linear, quadratic and second-order, respectively, K is the number of factors studied and e_i is the error. Analysis of variance based on the proposed model was performed to find the interaction between the response and the variable. The quality of the fit of the polynomial model was expressed by the determination coefficient (R^2) and the adjustment coefficient (R^2_{adj}).

2.4. Analytical methods

The morphology and elemental composition of the synthesized samples were determined by transmission electron microscopy (TEM) and SEM coupled with energy-dispersive X-ray spectroscopy (EDX). The crystalline structure of the samples was investigated by X-ray diffraction with Cu-K α radiation at a range of $2\theta = 10^\circ$ – 90° . The specific surface area of MMWCNTs was determined by the Brunauer–Emmett–Teller (BET) method. The chemical structure and functional groups of MMWCNTs were evaluated by Fourier transform infrared spectroscopy (FTIR) at a frequency range of 400–4,000 cm⁻¹. The zeta potential of the sample was measured with a zeta potential analyzer in aqueous solution.

The quantitative analysis of MFA and its intermediates were carried out using the DLLME/GC-MS method [32]. The electrogenerated H₂O₂ level was determined by titration with potassium permanganate. The MFA degradation efficiency (R) was calculated by Eq. (4).

$$R(\%) = \frac{C_i - C_f}{C_i} \times 100 \quad (4)$$

where C_i is the initial concentration of MFA, C_f is the final concentration of MFA, respectively. The reusability of

Table 1
Ranges of independent variables and their levels

Variables	Symbol	-2	-1	0	+1	+2
pH	X_1 or A	2.6	3.8	5	6.2	7.4
Initial MFA concentration (mg/L)	X_2 or B	2	4	6	8	10
Current density (mA/cm ²)	X_3 or C	5	10	15	20	25
Particle electrode concentration (mg/L)	X_4 or D	10	30	50	70	90
Electrolysis time (min)	X_5 or E	10	35	60	85	110

MMWCNTs was evaluated through five times repetition of the electro-oxidation process using the same electrodes.

3. Results and discussion

3.1. Characteristics of Ti/TiO₂-RuO₂

Fig. 1 shows the SEM images for Ti/TiO₂, Ti/RuO₂ and Ti/TiO₂-RuO₂ electrodes. According to this figure, all the synthesized anodes had flat surface and cracked-mud, which is common in metallic oxide anodes produced by thermal decomposition [33,34]. In Fig. 2, XRD analysis is shown from the surface of the substrate coated with titanium and ruthenium oxides. The main diffraction peaks around 25.7°, 38.05° and 48.40° were related to TiO₂ anatase [35]. While the diffraction peaks at 55.97°, 63.04°, 70.74° and

80.198° are related to titanium metal [36]. For analysis of Ti/RuO₂, the major diffraction peaks associated with RuO₂ were observed at 27.87°, 35° and 52.95° [35]. For the combined anode, TiO₂ and RuO₂ phases were present on the internal diagram of Fig. 2, which confirmed the formation of titanium metal oxide and ruthenium oxide phases.

3.2. Characteristics of MMWCNTs

Fig. 3 shows the morphology of the MWCNTs, Fe₃O₄ and MMWCNTs nanoparticles obtained by SEM. According to this figure, the surface structure of MWCNTs and Fe₃O₄ is obviously similar to tubes and spherical forms. Meanwhile, from the SEM image of MMWCNT, it can be seen that Fe₃O₄ nanoparticles are loaded onto the surface of the MWCNTs. In other words, it is clear that the magnetic nanoparticles

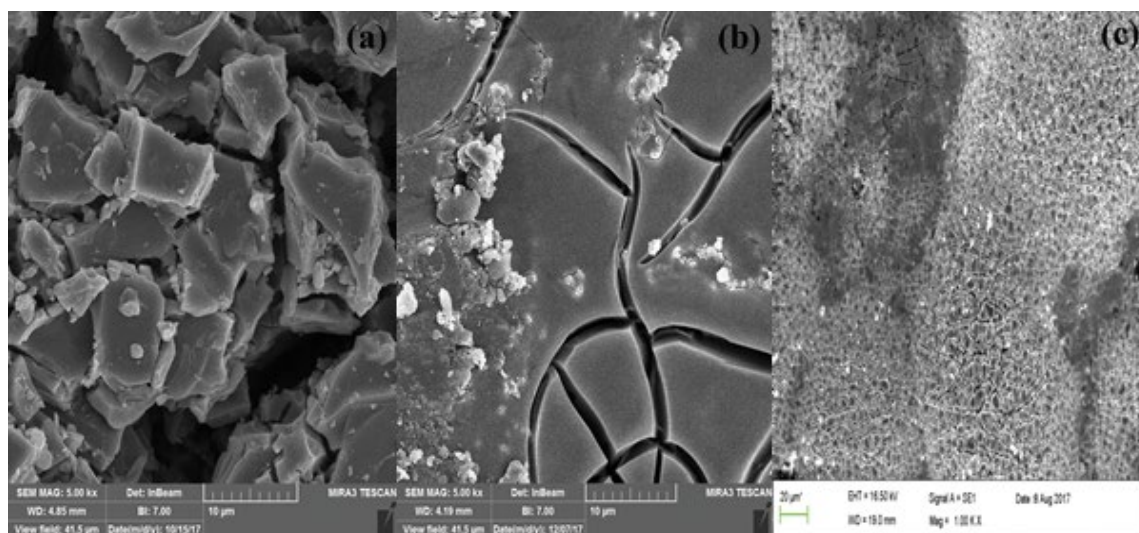


Fig. 1. SEM images of Ti/TiO₂ (a), Ti/RuO₂ (b), and Ti/TiO₂-RuO₂ (c) electrodes.

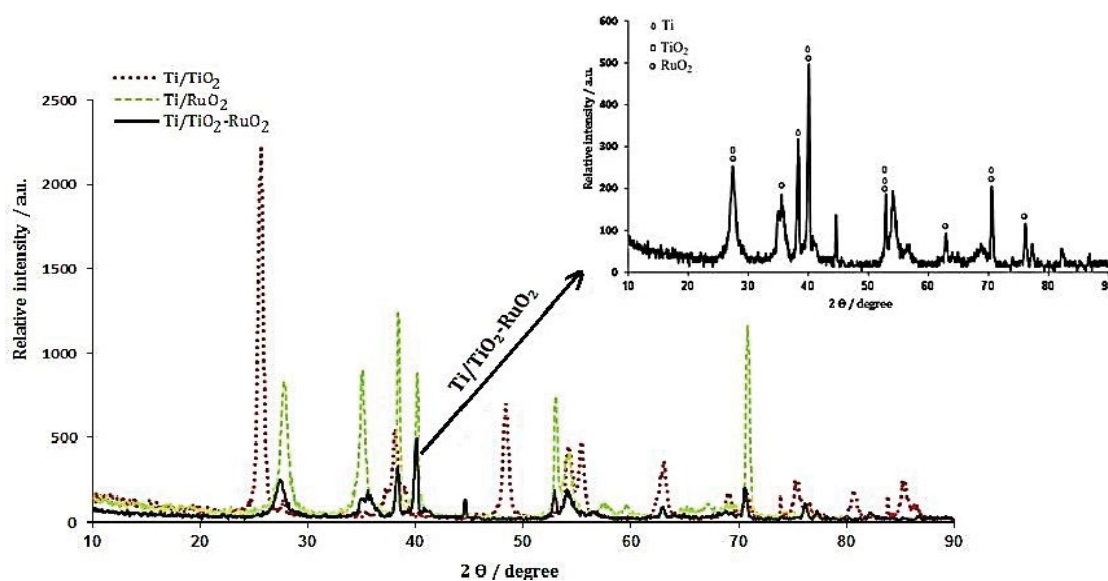


Fig. 2. XRD patterns of Ti/TiO₂ (a), Ti/RuO₂ (b), and Ti/TiO₂-RuO₂ (c) electrodes.

are irregularly attached to the outer wall of the MWCNT. Fig. 4 indicates the typical TEM image of the MMWCNTs electrode particle and the corresponding histogram to their size distribution. It can be seen from Fig. 4 that Fe_3O_4 nanoparticles with a range of 2–14 nm are coated in the form of black spots on the outer wall of CNTs.

The structure of the samples was evaluated by XRD analysis, and the results are shown in Fig. 5a. According to this figure, there are two diffraction peaks ($2\theta = 26.13^\circ$ and 44.5°) related to the structure of MWCNTs in the XRD pattern of MMWCNTs. For Fe_3O_4 , strong diffraction peaks occurred at $2\theta = 30^\circ, 35^\circ, 54^\circ, 57^\circ$ and 63° , which these peaks are clearly presented in the MMWCNTs structure. BET measurements showed that the BET surface areas of the MWCNTs and MMWCNTs particle electrodes were 122 and $228.51 \text{ m}^2/\text{g}$, respectively. These results emphasize that

Fe_3O_4 nanoparticles have been successfully coated on the MWCNTs surface.

Fig. 5b shows the FTIR spectra of MWCNTs, magnetic nanoparticles, and MMWCNTs. The peak absorption in the range $3,300\text{--}3,500 \text{ cm}^{-1}$ corresponds to the stretching vibrations of O–H. According to Saranya et al. [37], this peak in the magnetic nanoparticles, in addition to the hydroxyl functional group, can be due to water absorption in the sample. The absorption peaks at $2,800\text{--}2,900 \text{ cm}^{-1}$ are related to the asymmetric and symmetric stretching vibrations of CH_2 groups. The peak at $1,700 \text{ cm}^{-1}$ is related to the stretching vibrations of C=O, which indicates the adherence of carboxyl groups to the MWCNT surface. The absorption bands around $1,600 \text{ cm}^{-1}$ are related to the stretching vibration of the C=C and N–H groups. In spectra of MWCNT and MMWCNT peak was at $1,470 \text{ cm}^{-1}$ due to stretching

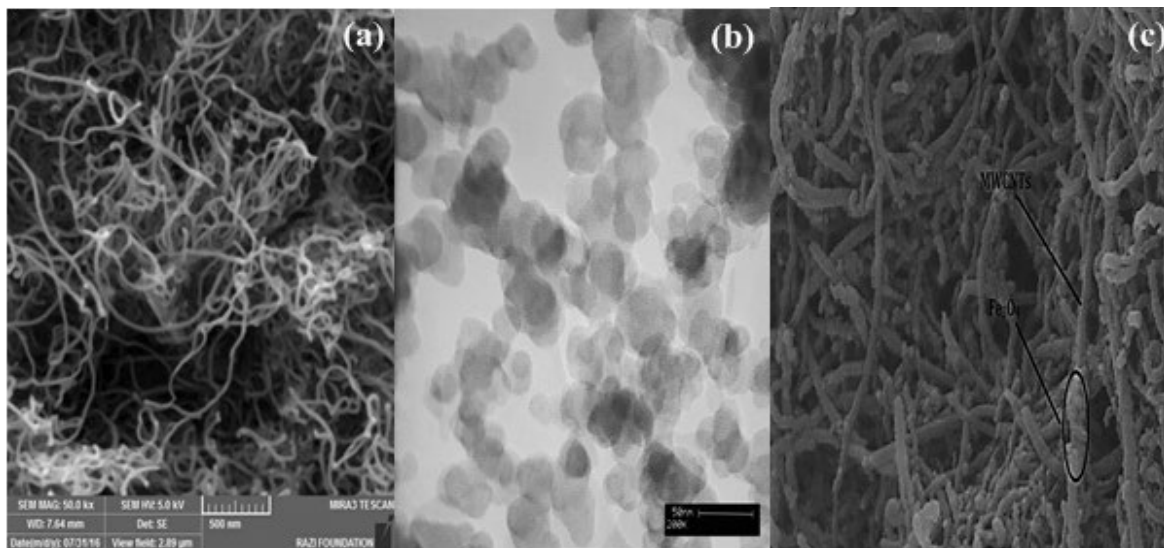


Fig. 3. SEM images of MWCNTs (a), magnetite (b), and MMWCNTs (c).

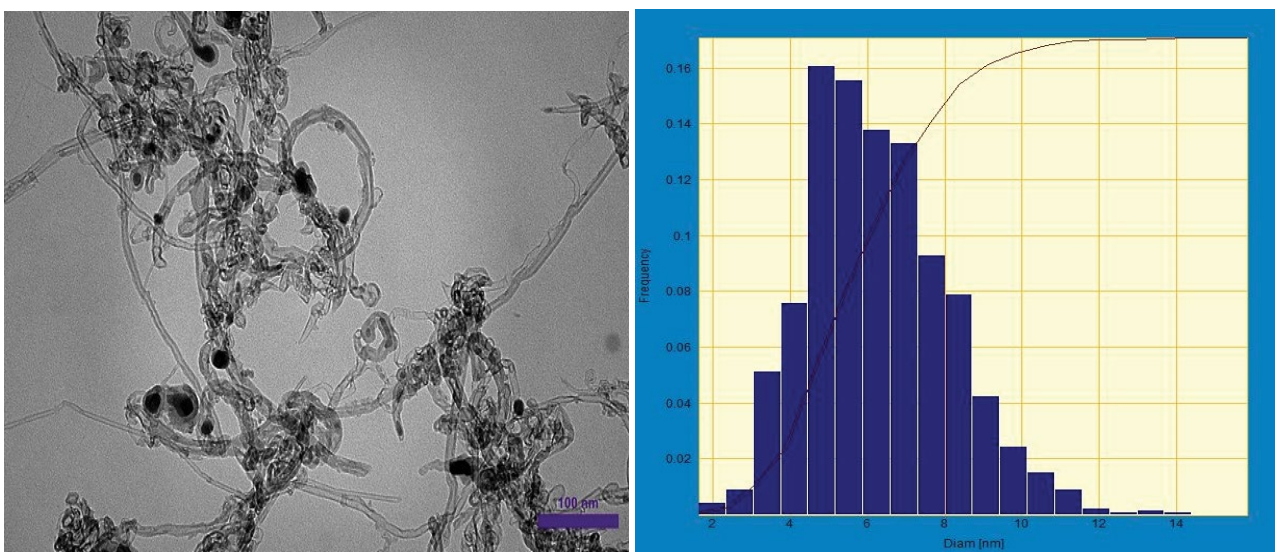


Fig. 4. TEM image and size distribution histogram of MMWCNTs.

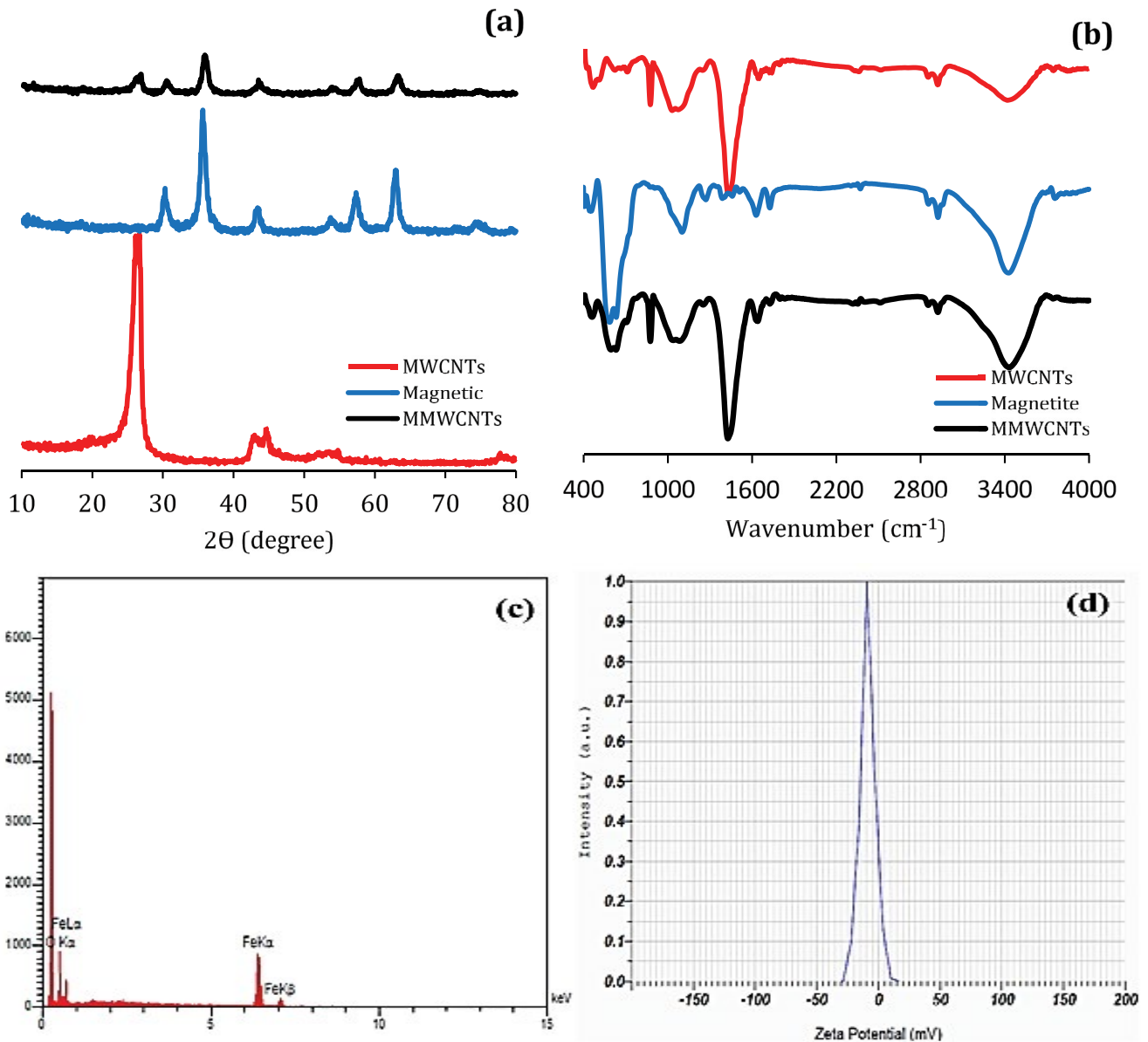


Fig. 5. XRD pattern (a), FTIR spectra (b), EDX pattern (c), and zeta potential (d) of synthesized catalysts.

vibration of C=O bond. The band at $1,010\text{ cm}^{-1}$ indicates a portion of the residual $-\text{OH}$, which can provide a good site for metals and organic compounds. The absorption peak at 570 cm^{-1} is related to the stretching vibration of Fe–O in the magnetic nanoparticles and MMWCNTs. The FTIR results confirmed that Fe_3O_4 has been successfully coated on the MWCNT surface using the co-precipitation method. To confirm the results of XRD and FTIR, the EDX spectrum (Fig. 5c) indicated the presence of Fe and O in the surface layer of the synthesized MMWCNTs.

According to studies, the net charge of nanocatalysts is one of the important parameters for their stability in the solution. Therefore, in this study, the zeta potential of the MMWCNTs was investigated, and the results were shown in Fig. 5d. As can be seen, the zeta potential of the particle

electrode synthesized by the co-precipitation method was 8.6 mV , which indicates that the MMWCNTs have a relatively small tendency for aggregation.

3.3. Preliminary investigations

It is well known that the crystalline nature of electrodes used can be strongly influenced by the electro-oxidation process [38]. Therefore, in the present study, the experiments were carried out to determine the MFA oxidation efficiency on Ti/TiO_2 , Ti/RuO_2 and $\text{Ti}/\text{TiO}_2\text{-RuO}_2$ under a pH of 3, MFA concentration of 10 mg/L , the current density of 10 mA/cm^2 , and airflow of 1 mL/min . The results in Fig. 6a show that the efficiency of the Ti/TiO_2 electrode was much lower than Ti/RuO_2 and $\text{Ti}/\text{TiO}_2\text{-RuO}_2$ electrodes. This may be due to the

low oxidation potential and high electrical resistance of Ti/TiO₂. Similar results were observed by Yue et al. [39] for electrochemical removal of nitrate.

Fig. 6b shows the electrochemical stability of Ti/RuO₂ and Ti/TiO₂-RuO₂ electrodes at pH of 3, MFA concentration of 10 mg/L, the current density of 10 mA/cm² and reaction time

of 60 min. According to this figure, the electrocatalytic activity of Ti/RuO₂ in the first 10 cycles was similar to Ti/TiO₂-RuO₂. However, by increasing the number of cycles from 10 to 20, the MFA degradation efficiency by Ti/RuO₂ decreases from 88.56% to 74.6%. In contrast, the MFA degradation efficiency with Ti/TiO₂-RuO₂ remains almost constant even after

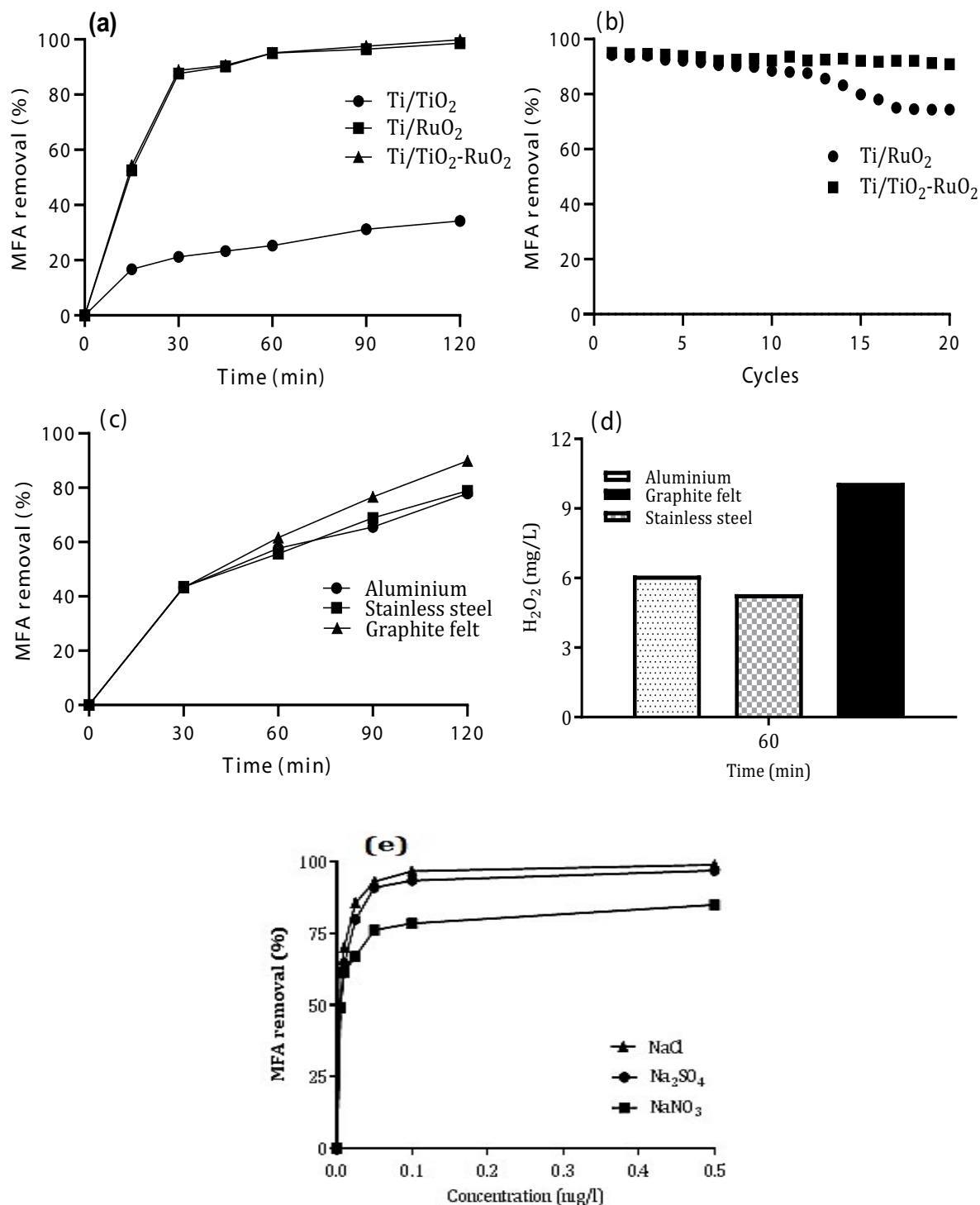


Fig. 6. (a) Electrocatalytic efficiency of the anode electrodes and (b) its electrochemical stability in the removal of MFA; (c) effect of cathode material on MFA removal and (d) electro-generation of H₂O₂; (e) effect of supporting electrolyte on removal MFA.

20 cycles. The high electrocatalytic activity and stability of Ti/TiO₂-RuO₂ can be due to the presence of TiO₂ and its effect on the development of RuO₂ mechanical stability during the electro-oxidation process [39].

Fig. 6c shows the effect of cathodic materials (graphite felt, aluminum, and stainless steel) on the degradation of MFA. As can be seen, graphite felt has a high MFA degradation rate and H₂O₂ production (Fig. 6d) compared with other cathodic materials (aluminum and stainless steel). This may be related to the high specific surface area of graphite felt, which can adsorb more soluble oxygen to produce H₂O₂ [25]. According to these results, Ti/TiO₂-RuO₂ and graphite felt were selected as anode and cathode electrodes, respectively, for subsequent experiments.

Supporting electrolyte is one of the most important factors in the electrochemical process due to the ability for improving solubility conductivity and accelerating the electron transfer. In this study, the effect of different types of electrolytes such as NaCl, Na₂SO₄ and NaNO₃ on the efficiency of the process was compared. As can be seen in Fig. 6e, the efficiency of NaCl and Na₂SO₄ in MFA decomposition was much higher than that of NaNO₃. This can be due to the high mobility of the ions of this salt. The results in Fig. 6e also show that initially by increasing the initial concentration of the supporting electrolyte from 0 to 0.05 M, the drug degradation efficiency was increased and then, the degradation rate remained constant as the electrolyte concentration increased. In the process of electro-oxidation, Na₂SO₄ is used as the most popular electrolyte due to the increasing current density and the lack of production of toxic and carcinogenic species such as chlorine and nitrate. Therefore, Na₂SO₄ with an initial concentration of 0.05 M was considered as a supporting electrolyte for the influence of other factors in the electro-oxidation process.

3.4. Response surface methodology study

In the design of the experiments, the RSM coupled with the CCD, as a suitable method for checking the experimental factors, reduces the number of designed tests required in the electrochemical process. Therefore, the effects and interaction of initial pH, current density, electrolysis time, MMWCNTs dosage and MFA concentration on the 3DEF process were evaluated by the design of experiments software and RSM. In this model, the backward algorithm was used to select the significant variables based on a *p*-value of less than 0.05. Based on the RSM results, the second-order polynomial equation between the response variable and the independent variables was expressed as follows.

$$\begin{aligned} \text{MFA degradation efficiency (\%)} = & 94.27 - 1.63X_1 + 3.57X_2 + \\ & 5.77X_3 + 5.75X_4 + 4.88X_5 + 0.91X_1X_2 + 1.05X_1X_3 + 0.88X_1X_4 + \\ & 0.44X_2X_3 - 3.04X_1^2 - 5.66X_2^2 - 3.41X_3^2 - 3.27X_4^2 - 3.43X_5^2 \end{aligned} \quad (5)$$

In this equation, the positive effect of a factor means that the efficiency of MFA degradation improves when the factor level increases, but the negative effect of a factor means that the efficiency does not improve when the factor level increases.

The statistical analysis of the model was performed by analysis of variance (ANOVA), and its results are shown

in Table 2. These results indicated a high *R*² (99.6%) for the degradation of MFA by the 3DEF process. This means that 99.6% of the variables for the MFA degradation efficiency can be explained by the model. The value of the adjusted coefficient of determination (*R*_{adj}² = 99.4) also confirms the high significance of the model. The low coefficient of variation (*C.V.* = 1.06) suggests high accuracy and reliability of the experiments. In addition, the *p*-value of less than 0.0001 and the *F* value of 676.84 indicate that the model is significant. Based on the *p*-value greater than 0.05, the lack of fit test of the final models was not significant, hence the fitting of the models confirmed that the final models are consistent with the experimental data. The adequate precision ratio for MFA degradation in the 3DEF process was obtained to be 98.89, which indicates a suitable signal for a quadratic model and the use of the model in the design space.

The effects of factors and interactions of MFA degradation efficiency using the 3DEF process (Table 2) showed that all main factors were significant. The results of Table 2 also shows the current density (*F* = 1,875.31) and the particle electrode concentration (*F* = 1,862.10) had the highest effect, and the initial pH (*F* = 149.61) had the least effect on the drug degradation. Fig. 7a confirms the ANOVA analysis results for the effect of factors. In this figure, the greater slope of the plot represents the importance of the factor in the process. These results also were confirmed by the results of the Pareto chart (Fig. 7b). In addition, the results of Table 2 showed that the effects of interactions were generally lower than the main factors, among which the interactions of *AB*, *AC*, *AD* and *BC* were significant. Fig. 8 confirms the ANOVA analysis results for the interaction of factors. In this figure, the parallel lines mean that there is no interaction between the two variables, while the crossings lines indicate the interactions between the variables. Among the second-order interactions, all interactions were significant, and the greatest effect on degradation of MFA was observed for interaction between initial concentration of the drug and the initial concentration of the drug (*B*²) due to the high *F*-value.

Based on the results of the interaction represented in Table 2 and Fig. 8, it can be concluded that in the low and high limits of the initial concentration of the drug (*B*), the current density (*C*) and the initial amount of the particle electrode (*D*), the MFA degradation efficiency is initially increased by increasing the pH (*A*), and is then reduced. In addition, MFA degradation at low and high limits of current density (*C*) initially increases with an increase in initial concentration, then decreases. These results emphasize that in high levels of factors, a good degradation efficiency of MFA can be achieved at its different concentrations. The 3D plots (Fig. 9), in addition to confirming these results, showed that in high current densities and particle electrode concentrations, the efficiency obtained is approximately similar in the pH range of 3.8 to 6.2.

In order to verify the adequacy of the model, the diagnostic plots shown in Fig. 10 were used. As can be seen, the predicted plots data are in good agreement with experimental data. The straight line in Fig. 10b showed that the residuals with uniform scattering had a normal distribution. The results of Figs. 10c and d showed that about half the residuals are higher and the other half lower than the zero lines, which indicates that all of the residuals are close to zero and there is

Table 2
ANOVA results for the quadratic model of MFA removal using 3DEF process

Source	Sum of squares	df	Mean square	F value	p-value (Prob > F)
Model	6,726.73	14	480.48	676.84	<0.0001
A-pH	106.21	1	106.21	149.61	<0.0001
B-MFA concentration (mg/L)	509.92	1	509.92	718.31	<0.0001
C-current density (mA/cm ²)	1,331.26	1	1,331.26	1,875.31	<0.0001
D-MMWCNTs concentration (mg/L)	1,321.89	1	1,321.89	1,862.10	<0.0001
E-electrolysis time (min)	953.89	1	953.89	1,343.71	<0.0001
AB	26.76	1	26.76	37.70	<0.0001
AC	35.35	1	35.35	49.80	<0.0001
AD	24.84	1	24.84	34.99	<0.0001
BC	6.09	1	6.09	8.57	0.0060
A ²	296.09	1	296.09	417.09	<0.0001
B ²	1,023.60	1	1,023.60	1,441.92	<0.0001
C ²	371.29	1	371.29	523.03	<0.0001
D ²	342.80	1	342.80	482.90	<0.0001
E ²	376.75	1	376.75	530.71	<0.0001
Residual	24.85	35	0.71		
Lack of fit	21.81	28	0.78	1.80	0.2158
Pure error	3.03	7	0.43		
Cor total	6,751.58	49			
R ²	0.996				
Adjusted R ²	0.994				
Predicted R ²	0.991				
Adequate precision	98.89				
C.V. %	1.06				

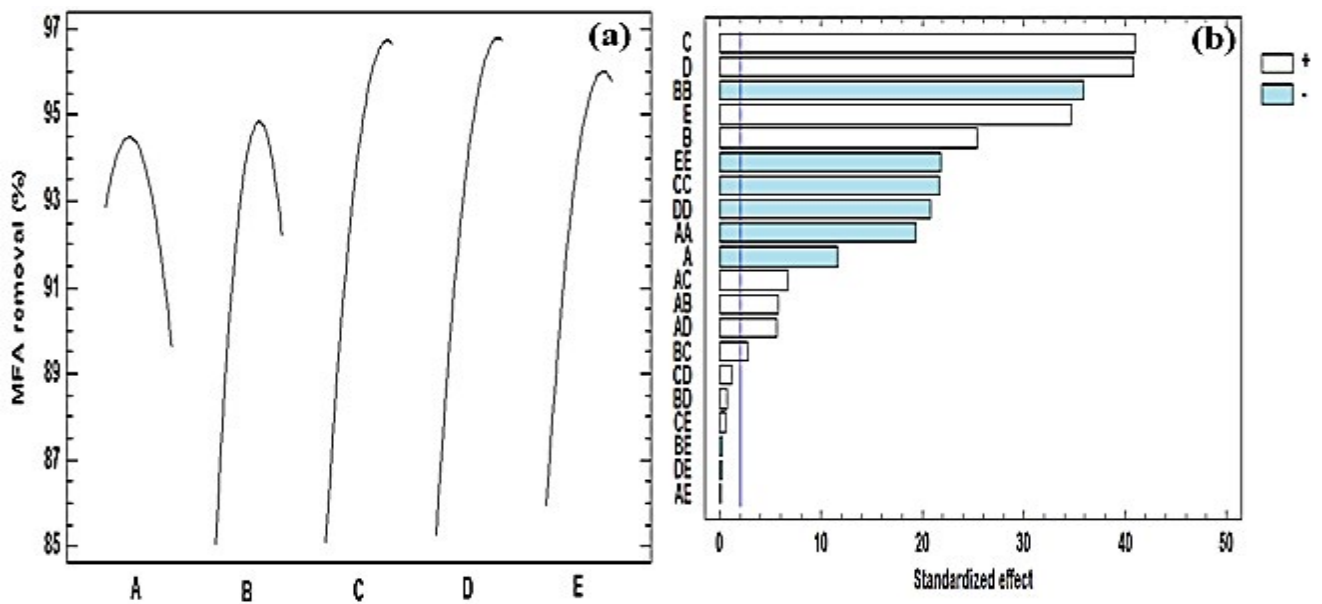


Fig. 7. (a) Main effects plot and (b) Pareto chart standardized for showing the effect of all factors on MFA removal.

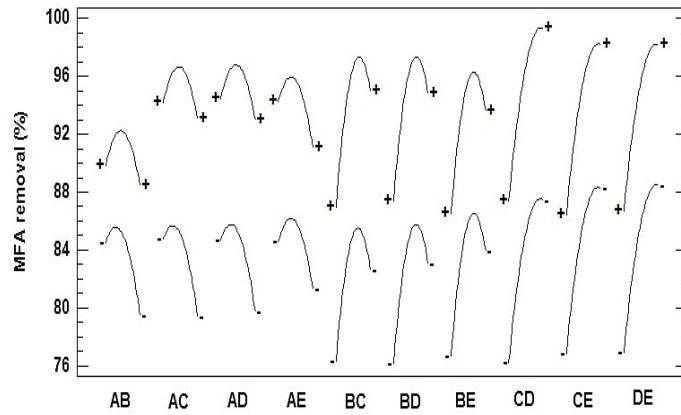


Fig. 8. Interaction plots for MFA removal efficiency ((A) pH; (B) MFA concentration; (C) current density; (D) concentration of MMWCNTs; (E) reaction time).

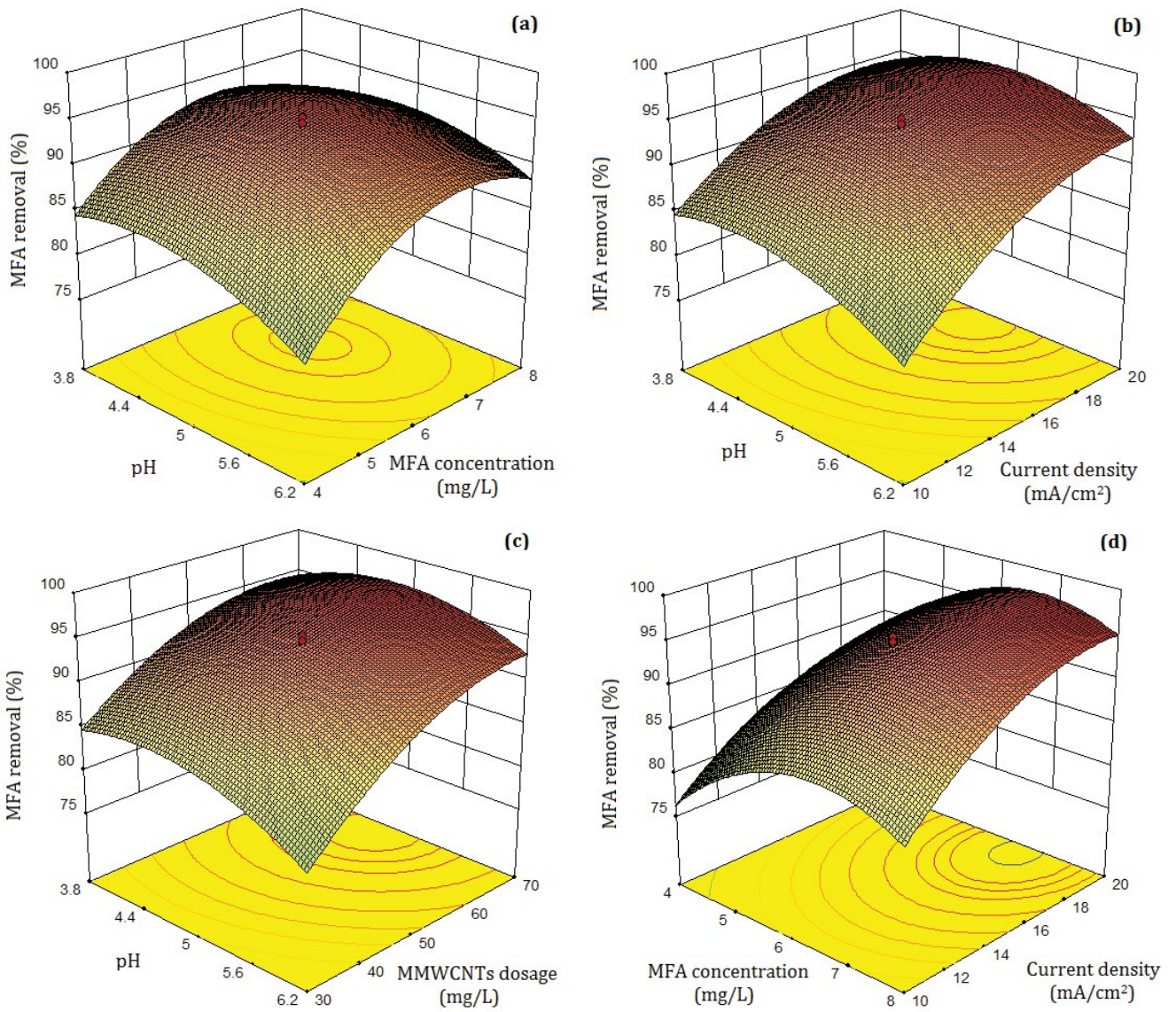


Fig. 9. 3D surface plots showing the interaction of different experimental parameters.

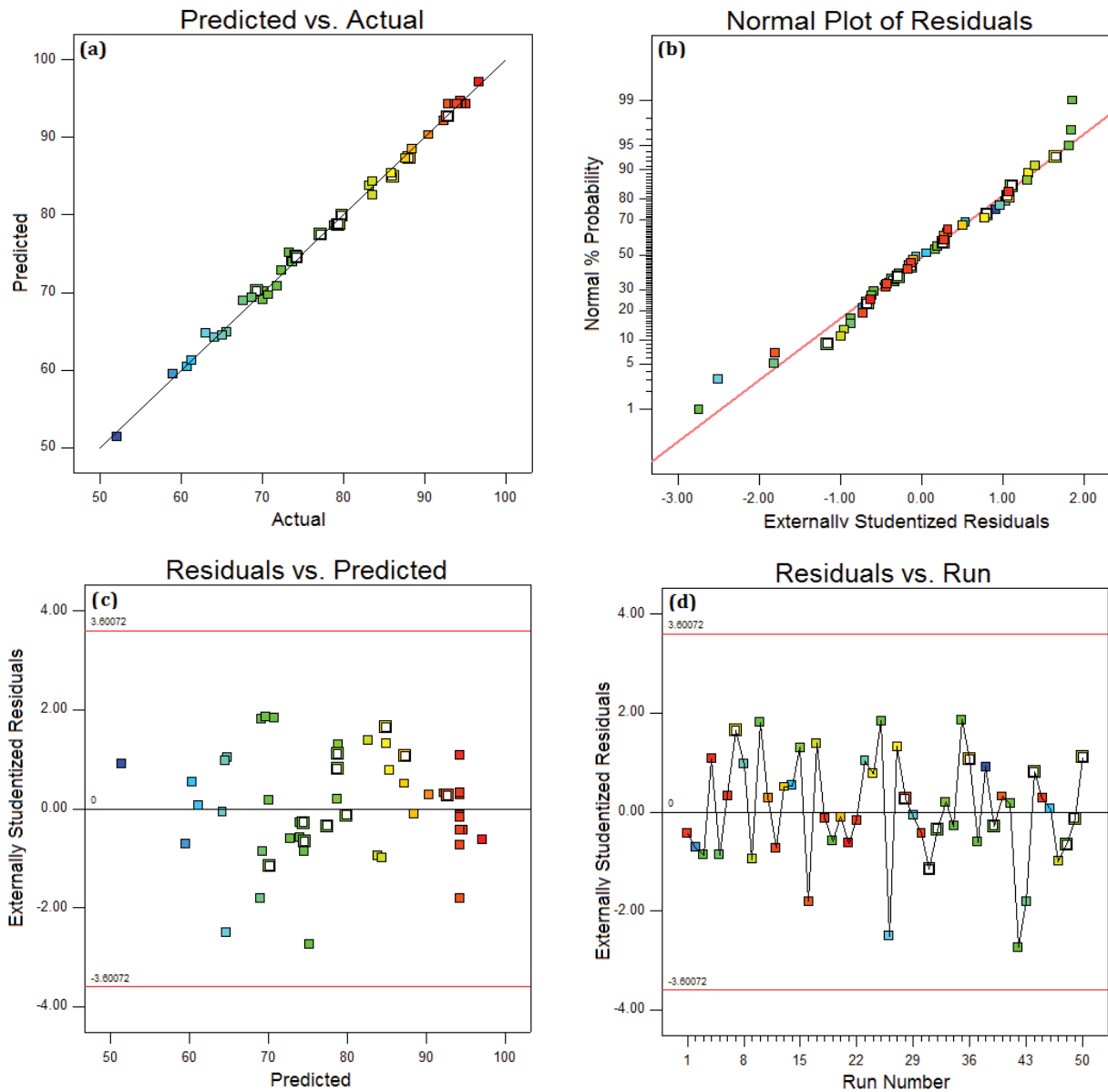


Fig. 10. (a) Predicted vs. actual values plot, (b) normal probability plot, (c) residual vs. predicted plot and (d) Studentized residuals vs. run number plot for MFA removal.

less error for predicted degradation efficiency. According to these results, it can be concluded that the obtained model is sufficient to explain the relationship between MFA degradation efficiency and operational factors.

3.5. Effect of operational parameters

3.5.1. Initial pH

Initial pH values play an important role in the formation of reactive species (such as H_2O_2 and $\cdot OH$), their stability and oxidation potential in electro-oxidation systems [21]. Fig. 7a depicts the effect of pH on the MFA degradation efficiency under conditions including MFA concentration of 6 mg/L, the current density of 15 mA/cm², MMWCNTs dosage of

50 mg/L and the electrolysis time of 60 min. As can be seen, the MFA degradation rate at pH values of 3.8, 5.6 and 6.2 was 92.9%, 94.33% and 89.68%, respectively. These results suggest that the electro-Fenton process coupled with MMWCNTs has an appropriate efficiency within the pH range of the study. This trend is attributed to reducing the pH effect on the Fenton reaction due to the excellent electrical conductivity, adsorption and catalytic properties of MMWCNTs [40]. In addition, MWCNTs, by absorbing oxygen and its electro-chemical reduction, produce H_2O_2 and subsequently $\cdot OH$ within the pH range of the study [32]. Mohammadi et al. [41] observed similar results in the degradation of naproxen and ibuprofen. They reported that the chelating of Fe with the support material prevents the formation of $Fe(OH)_3$ and eliminates the negative effect of the iron sludge produced in

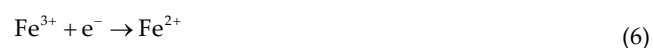
the electro-Fenton process. In addition, similar results were reported by Zhang et al. [18] and Tang et al. [42], for the degradation of rhodamine B and p-nitrophenol, respectively.

3.5.2. Initial concentration of MFA

To evaluate the effect of the initial concentration of MFA on the electrocatalytic activity of the 3DEF process, various concentrations of MFA (4–8 mg/L) were tested, and the results are shown in Fig. 7a. As can be seen, when the MFA concentration rises from 4 to 6 mg/L, the degradation efficiency significantly increases from 84.9% to 94.6%. While, with a further increase in the MFA to 8 mg/L, the efficiency reduces to 92.1%. The initial increase in efficiency can be due to the greater accessibility of MFA molecules to $\cdot\text{OH}$ during the 3DEF process. Similar results were reported by Manu and Mahamood [43] for the degradation of diclofenac by the Fenton process. Reducing the efficiency could be related to the inaccessibility of active sites of MMWCNTs for generating the reactive species due to their occupation by the main pollutant and the intermediates produced by its oxidation. Similar results were observed by He et al. [21] for the degradation of reactive blue 19. Efficiency decrease at high concentrations was explained based on the inadequacy of produced $\cdot\text{OH}$ and the low $\text{Fe}^{2+}/\text{Fe}^{3+}$ active sites for H_2O_2 decomposition.

3.5.3. Current density

The current density is one of the most important operational parameters on the efficiency of the 3D process due to its effect on electrochemical oxidation, the polarization behavior of particle electrodes and the production of H_2O_2 through the reduction of oxygen on the surface of the electrodes. The degradation efficiency of MFA by the 3DEF process at different current densities is shown in Fig. 7a. According to this figure, with an increase in the current density from 10 to 18 mA/cm², the degradation efficiency of MFA was increased from 85.75% to 96.83%. While, by further increasing the current density from 18 to 20 mA/cm², the MFA degradation efficiency remains constant. The initial increase in efficiency may be related to the more production of $\cdot\text{OH}$ through the effect of high current density on the production of H_2O_2 (Eq. (1)) and the faster regeneration of iron ions at the cathode surface (Eq. (6)) [40]. In addition, by increasing the current density, MFA molecules are further adsorbed onto the main electrodes and MMWCNTs, thus the collision between $\cdot\text{OH}$ and MFA molecules is enhanced [44]. At an appropriate current, MWCNTs are also polarized in the form of numerous microelectrodes, which improve the electrosorption and oxidation processes. The fixed efficiency at the high current densities can be related to hydroperoxyl radical ($\text{HOO}\cdot$) production (Eq. (7)) through the reaction between $\cdot\text{OH}$ with an excess of H_2O_2 . According to He et al. [21], $\text{HOO}\cdot$ radical has lower oxidation potential compared with $\cdot\text{OH}$, which leads to decreasing or fixing the efficiency at high current densities. Similar results were observed by Es'haghzade et al. [45] for the degradation of azo dyes from aqueous solutions.



3.5.4. MMWCNTs dosage

The amount of particle electrode is another important parameter in the 3D processes due to its major role in adsorption and H_2O_2 electrochemical production. Fig. 7a shows the efficiency of MFA degradation in the presence of a different amount of MMWCNTs. It can be seen that by increasing the amount of particle electrode from 30 to 65 mg/L, the degradation efficiency of MFA increases from 85.29% to 96.72%. But in the presence of the particle electrode values higher than 65 mg/L, the efficiency of the 3DEF process remains constant. The initial increase in the efficiency could be related to an increase in the number of active sites on the MMWCNTs surface, and subsequently acceleration of H_2O_2 decomposition into $\cdot\text{OH}$ and an increase in the amount of iron ion released into the solution. Fixed efficiency can be due to the consumption of $\cdot\text{OH}$ by excessive ferrous ion and the occupation of the surface of the cathode by ferric ion. Similar results were reported by Zhang et al. [15] and Ozcan et al. [46] in terms of increasing the pollutants removal efficiency by an initial increase in the catalyst dosage and then reducing the efficiency by its further increase.

3.5.5. Time of electrolysis

Fig. 7a shows the effect of electrolysis time on the MFA degradation efficiency at pH of 5, MFA concentration of 6 mg/L, the current density of 15 mA/cm² and MMWCNTs dosage of 50 mg/L. According to this figure, with an increase in the electrolysis time from 35 to 75 min, the MFA degradation efficiency increases. This can be due to the formation of more $\cdot\text{OH}$ on the surface of Ti/TiO₂-RuO₂ and the production of more H_2O_2 on the surface of the cathode and particle electrode. Similar results were observed by Pourzamani et al. [47] for the degradation of ciprofloxacin from aqueous solution. The greater increase in the reaction time from 75 to 85 min reduces the efficiency of the 3DEF process. This is due to the occupation of the cathode pores and the particle electrode by the intermediates produced from MFA degradation and the reduction of H_2O_2 production. These results are consistent with results reported by Nidheesh et al. [44] for the degradation of rhodamine B using electro-Fenton catalyzed by Fe_3O_4 .

3.6. Optimization of the 3DEF process

To validate and confirm the prediction model, the optimization performed by Design-Expert 10 software showed that the maximum MFA degradation efficiency (98.36%) can be obtained at the pH of 6.2, MFA concentration of 6.19 mg/L, current density of 19.94 mA/cm², MMWCNTs dosage of 69.13 mg/L and the reaction time of 82.95 min. To confirm the reliability, several experiments were performed using predicted optimum conditions. The average degradation efficiency of the experimental results (98.89%) was in good agreement with the predicted results, which confirms that the model designed in this study was sufficient.

3.7. Electrocatalytic performance of the 3DEF process

To understand the efficiency of the MMWCNTs electrode particle in the 3DEF system, the COD removal efficiency in

various systems was examined and the results are shown in Fig. 11a. As can be seen, the removal efficiency obtained by the process without current density was 16.16%, which indicates that the MFA adsorption by the catalyst was negligible because of the low amounts of MMWCNTs used in the reaction. In addition, the removal efficiency of the two dimensional electrochemical (2DE) process was 35.42% in 90 min. In contrast, the COD removal efficiency by the homogenous electro-Fenton (EF) process was 53.5% at the same time. This increased efficiency in the EF system can be due to the more production of $\cdot\text{OH}$ in the anode surface and the reaction of Fenton in the solution. Compared with the above-mentioned process, COD removal efficiency obtained by electrochemical processes coupled with MWCNT and MMWCNTs was 75.55% and 90.9%, respectively. This high efficiency in 3D processes may be due to the role of the MWCNT particle electrode in adsorption of pollutant, the development of electrocatalytic reactions and increasing the production of reactive species. Similar results were observed by Pourzamani et al. [47] for the degradation of ciprofloxacin.

Along with the removal of COD, the concentration of H_2O_2 was similarly evaluated. As can be seen in Fig. 11b, the amount of H_2O_2 produced in the electrocatalytic process containing MWCNT was greater than the 2DE and EF processes. This could be related to the ability of MWCNT for the electrochemical reduction of O_2 to H_2O_2 . The results of Fig. 11b also show that the production of H_2O_2 in the 3DEF process was lower than the electrolysis process containing MWCNT. This can be due to the rapid decomposition of H_2O_2 into reactive species in the presence of iron ions. According to these results, the 3DEF process can provide higher COD removal efficiency and higher $\cdot\text{OH}$ production compared with other systems.

In addition to the above observations, the MFA degradation efficiency by the 3DEF system has been compared with other reported oxidation processes in previous studies and, its results are reported in Table 3. As can be seen, the MFA

degradation efficiency by the MMWCNTs-based 3DEF system is higher compared with the other oxidation processes, and less electrolysis time is required at pH values near neutral. Table 3 also shows that MMWCNTs have the same catalytic performance compared with other catalysts used in the heterogeneous electro-Fenton process. Therefore, the 3DEF system coupled with MMWCNTs can be used as a new electrocatalyst for MFA degradation.

3.8. Stability and reusability of the MMWCNTs

The stability of the MMWCNTs particle electrode was evaluated by five consecutive experiments of MFA oxidation under the same reaction conditions (pH = 6.2, MFA concentration = 6.19 mg/L, current density = 19.94 mA/cm², MMWCNTs = 69.13 mg/L and reaction time = 90 min). The results showed that the particle electrode could be successfully recycled for five consecutive cycles with degradation efficiency of more than 94%, which confirms the good recycling and stability of the particle electrode (Fig. 12). However, the COD removal efficiency significantly decreases during the five reaction cycles, which can be attributed to the extra production of byproducts and the occupation of the active sites of MMWCNTs by them. Similar results were obtained by Tang et al. [42] for the degradation of methyl orange.

3.9. Degradation pathways of MFA

The identified byproducts and possible reaction pathways for the electro-oxidation degradation of MFA are shown in Table 4 and Fig. 13. Based on the electro-oxidation mechanism, the MFA is initially oxidized to 2-[(2,3-dimethylphenyl)amino]-benzoic acid through the loss of hydrogen. Riyanto and Anshori [51] obtained the same results and reported that MFA is oxidized to 2-[(2,3-dimethylphenyl)amino] benzoic acid through the loss of an electron and hydrogen. After this, by attacking the $\cdot\text{OH}$ on the C–N

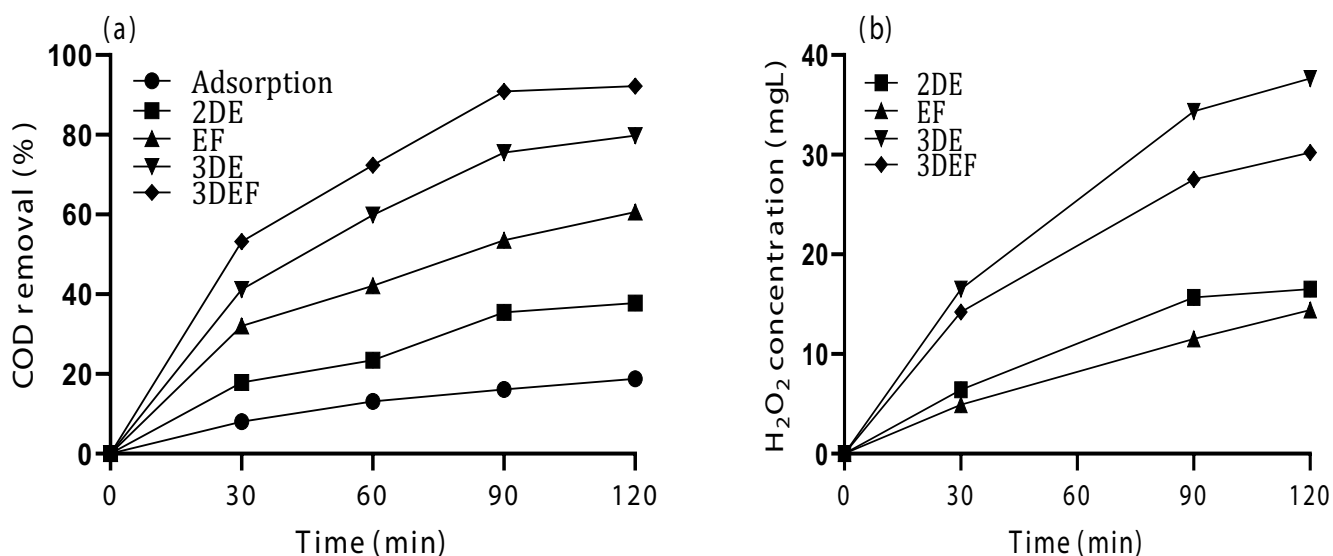


Fig. 11. (a) Removal efficiency of COD and (b) H_2O_2 electrochemical production (pH = 6.2, MFA concentration = 6.19 mg/L, current density = 19.94 mA/cm², MMWCNTs dosage = 69.13 mg/L).

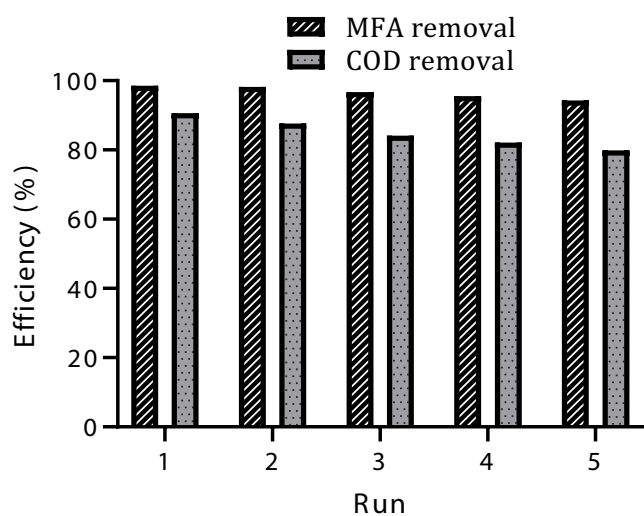


Fig. 12. Stability of the MMWCNTs in MFA and COD removal experiments.

bond and the breakdown of the aromatic rings of MFA and 2-[(2,3-dimethylphenyl) amino] benzoic acid, the compounds such as 3,4-dimethyl benzaldehyde and 3-methylbut-2-enoic acid is formed. These results are in agreement with the Khalit and Tay [52] for the degradation of MFA by chlorination.

4. Conclusions

In the present study, MMWCNTs were used as a novel particle electrode in the 3DEF process for the degradation of MFA from aqueous solutions. The five levels of the central composite design were assessed for the evaluation and optimization of the five important operational parameters. Among them, the ANOVA analysis and proposed quadratic model showed that the current density, due to the effect on the development of direct and indirect catalytic oxidation at the catalyst surface, is the most important parameter. The high values of R^2 , adjusted R^2 , and predicted R^2 showed that the quadratic model was well fitted with the

Table 3
Comparison of the MMWCNTs based 3DEF system with other oxidation processes

Processes	Pollutant	Condition	Efficiency (%)	Reference
Photo-Fenton	MFA	pH: 6.1, Catalyst: 1 m/moL, H ₂ O ₂ : 17.5 mmol, time: 60 min	95	[8]
Photocatalytic	MFA	pH: 4, catalyst: 1 g/L, T: 160 min	≈65%	[48]
Heterogeneous EF	Diuron	pH: 6.7, current: 100 mA, catalyst: 3 g/L, time: 100 min	95%	[49]
Heterogeneous EF	p-Nitrophenol	pH: 3, current density: 3 mA/cm ² , pollutant concentration: 50 mg/L; catalyst: 3 g/L, time: 60 min	94.31%	[42]
Heterogeneous EF	2,4-Dichlorophenol	pH: 6.7, current: 100 mA, pollutant concentration: 120 mg/L; catalyst: 6 g/L, time: 120 min	95%	[50]
3DEF	MFA	pH: 6.2, current density: 19.94 mA/cm ² , pollutant concentration: 6.19 mg/L; catalyst: 69.13 mg/L, time: 82.95 min	98.89%	This study

Table 4
Intermediates detected by GC-MS during degradation of MFA

structure	Retention time (min)	MW	Name	Formula	m/z	Prob. (%) in NIST library
	21.45	255.31	Benzoic acid, 2-[(2,3-dimethylphenyl)amino]-	C ₁₆ H ₁₇ NO ₂	223	41
	9.164	100.11	3-Methylbut-2-enoic acid	C ₅ H ₈ O ₂	100	28
	10.58	134.17	3,4-Dimethyl benzaldehyde	C ₉ H ₁₀ O	133–134	64

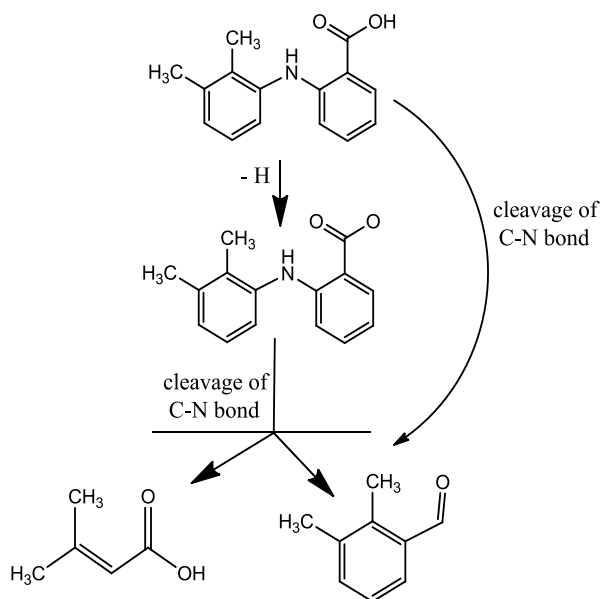


Fig. 13. Possible pathway for degradation of MFA by the 3DEF reactor.

experimental data. The optimal condition for the maximum degradation efficiency of MFA (98.36%) was obtained at pH of 6.2, MAF concentration of 6.19 mg/L, the current density of 19.24 mA/cm², MMWCNTs dosage of 69.63 mg/L and reaction time of 82.95 min. Comparative experiments between different electro-oxidation processes demonstrated the high electrocatalytic activity and more production of reactive species in the 3DEF process. This may be due to the formation of a large number of charged microelectrodes to improve the direct and indirect oxidation mechanism. The electrocatalytic stability of MMWCNTs showed a good recycling capacity for the long-term electrocatalytic degradation of MFA. Three main MFA degradation intermediates were identified by DLLME and GC-MS analysis, and the electrochemical degradation pathway was proposed for the byproducts. Finally, the results showed that the 3DEF process catalyzed with MMWCNTs could be considered as a promising alternative method for conventional oxidation processes due to its high efficiency, stability, and reusability of the electrode particle.

Acknowledgment

This work was supported by the Isfahan University of Medical Sciences (No. 395729).

References

- [1] J.-L. Liu, M.-H. Wong, Pharmaceuticals and personal care products (PPCPs): a review on environmental contamination in China, *Environ. Int.*, 59 (2013) 208–224.
- [2] Y.F. Velázquez, P.M. Nacheva, Removal of pharmaceuticals from municipal wastewater by aerated submerged attached growth reactors, *J. Environ. Manage.*, 192 (2017) 243–253.
- [3] L. Feng, E.D. Van Hullebusch, M.A. Rodrigo, G. Esposito, M.A. Oturan, Removal of residual anti-inflammatory and analgesic pharmaceuticals from aqueous systems by electrochemical advanced oxidation processes. A review, *Chem. Eng. J.*, 228 (2013) 944–964.
- [4] E. Chang, T.-Y. Liu, C.-P. Huang, C.-H. Liang, P.-C. Chiang, Degradation of mefenamic acid from aqueous solutions by the ozonation and O₃/UV processes, *Sep. Purif. Technol.*, 98 (2012) 123–129.
- [5] A. Eslami, M.M. Amini, A.R. Yazdanbakhsh, N. Rastkari, A. Mohseni-Bandpei, S. Nasser, E. Piroti, A. Asadi, Occurrence of non-steroidal anti-inflammatory drugs in Tehran source water, municipal and hospital wastewaters, and their ecotoxicological risk assessment, *Environ. Monit. Assess.*, 187 (2015) 734.
- [6] H. Abdolmohammad-Zadeh, F. Morshedzadeh, E. Rahimpour, Trace analysis of mefenamic acid in human serum and pharmaceutical wastewater samples after pre-concentration with Ni–Al layered double hydroxide nano-particles, *J. Pharm. Anal.*, 4 (2014) 331–338.
- [7] J.J. Werner, K. McNeill, W.A. Arnold, Environmental photodegradation of mefenamic acid, *Chemosphere*, 58 (2005) 1339–1346.
- [8] R. Colombo, T.C. Ferreira, R.A. Ferreira, M.R. Lanza, Removal of Mefenamic acid from aqueous solutions by oxidative process: optimization through experimental design and HPLC/UV analysis, *J. Environ. Manage.*, 167 (2016) 206–213.
- [9] D. Kanakaraju, B.D. Glass, M. Oelgemöller, Advanced oxidation process-mediated removal of pharmaceuticals from water: a review, *J. Environ. Manage.*, 219 (2018) 189–207.
- [10] K. Ikehata, N. Jodeiri Naghashkar, M. Gamal El-Din, Degradation of aqueous pharmaceuticals by ozonation and advanced oxidation processes: a review, *Ozone Sci. Eng.*, 28 (2006) 353–414.
- [11] S. Ghasemian, D. Nasuhoglu, S. Omanovic, V. Yargeau, Photoelectrocatalytic degradation of pharmaceutical carbamazepine using Sb-doped Sn_{80%}-W_{20%}-oxide electrodes, *Sep. Purif. Technol.*, 188 (2017) 52–59.
- [12] R. Banaschik, H. Jablonowski, P.J. Bednarski, J.F. Kolb, Degradation and intermediates of diclofenac as instructive example for decomposition of recalcitrant pharmaceuticals by hydroxyl radicals generated with pulsed corona plasma in water, *J. Hazard. Mater.*, 342 (2018) 651–660.
- [13] P. Duan, X. Hu, Z. Ji, X. Yang, Z. Sun, Enhanced oxidation potential of Ti/SnO₂-Cu electrode for electrochemical degradation of low-concentration ceftazidime in aqueous solution: performance and degradation pathway, *Chemosphere*, 212 (2018) 594–603.
- [14] F.C. Moreira, R.A. Boaventura, E. Brillas, V.J. Vilar, Electrochemical advanced oxidation processes: a review on their application to synthetic and real wastewaters, *Appl. Catal., B*, 202 (2017) 217–261.
- [15] C. Zhang, M. Zhou, G. Ren, X. Yu, L. Ma, J. Yang, F. Yu, Heterogeneous electro-Fenton using modified iron-carbon as catalyst for 2, 4-dichlorophenol degradation: influence factors, mechanism and degradation pathway, *Water Res.*, 70 (2015) 414–424.
- [16] L. Labiadh, M.A. Oturan, M. Panizza, N.B. Hamadi, S. Ammar, Complete removal of AHPs synthetic dye from water using new electro-Fenton oxidation catalyzed by natural pyrite as heterogeneous catalyst, *J. Hazard. Mater.*, 297 (2015) 34–41.
- [17] E. Brillas, I. Sirés, M.A. Oturan, Electro-Fenton process and related electrochemical technologies based on Fenton's reaction chemistry, *Chem. Rev.*, 109 (2009) 6570–6631.
- [18] B. Zhang, Y. Hou, Z. Yu, Y. Liu, J. Huang, L. Qian, J. Xiong, Three-dimensional electro-Fenton degradation of Rhodamine B with efficient Fe-Cu/kaolin particle electrodes: electrodes optimization, kinetics, influencing factors and mechanism, *Sep. Purif. Technol.*, 210 (2019) 60–68.
- [19] H. Chen, Y. Feng, N. Suo, Y. Long, X. Li, Y. Shi, Y. Yu, Preparation of particle electrodes from manganese slag and its degradation performance for salicylic acid in the three-dimensional electrode reactor (TDE), *Chemosphere*, 216 (2019) 281–288.
- [20] F. Iranpour, H. Pourzamani, N. Mengelizadeh, P. Bahrami, H. Mohammadi, Application of response surface methodology for optimization of reactive black 5 removal by three

- dimensional electro-Fenton process, *J. Environ. Chem. Eng.*, 6 (2018) 3418–3435.
- [21] Z. He, C. Gao, M. Qian, Y. Shi, J. Chen, S. Song, Electro-Fenton process catalyzed by Fe_3O_4 magnetic nanoparticles for degradation of CI Reactive Blue 19 in aqueous solution: operating conditions, influence, and mechanism, *Ind. Eng. Chem. Res.*, 53 (2014) 3435–3447.
- [22] C. Zhang, M. Zhou, G. Ren, X. Yu, L. Ma, J. Yang, F. Yu, Heterogeneous electro-Fenton using modified iron-carbon as catalyst for 2,4-dichlorophenol degradation: Influence factors, mechanism and degradation pathway, *Water Res.*, 70 (2015) 414–424.
- [23] N. Qiao, H. Ma, M. Hu, Design of a neutral three-dimensional electro-Fenton system with various bentonite-based Fe particle electrodes: a comparative study, *Mater. Res. Innov.*, 19 (2015) S2–137–S132–141.
- [24] H.-Y. Xu, Y. Wang, T.-N. Shi, H. Zhao, Q. Tan, B.-C. Zhao, X.-L. He, S.-Y. Qi, Heterogeneous Fenton-like discoloration of methyl orange using $\text{Fe}_3\text{O}_4/\text{MWCNTs}$ as catalyst: combination mechanism and affecting parameters, *Front. Mater. Sci.*, 12 (2018) 21–33.
- [25] H. Pourzamani, N. Mengelizadeh, Y. Hajizadeh, H. Mohammadi, Electrochemical degradation of diclofenac using three-dimensional electrode reactor with multi-walled carbon nanotubes, *Environ. Sci. Pollut. Res.*, 25 (2018) 24746–24763.
- [26] H. Lee, H.-J. Lee, J. Jeong, J. Lee, N.-B. Park, C. Lee, Activation of persulfates by carbon nanotubes: oxidation of organic compounds by nonradical mechanism, *Chem. Eng. J.*, 266 (2015) 28–33.
- [27] X. Zhang, M. Feng, R. Qu, H. Liu, L. Wang, Z. Wang, Catalytic degradation of diethyl phthalate in aqueous solution by persulfate activated with nano-scaled magnetic $\text{CuFe}_2\text{O}_4/\text{MWCNTs}$, *Chem. Eng. J.*, 301 (2016) 1–11.
- [28] S.M. El-Khouly, N.A. Fathy, Multi-walled carbon nanotubes supported amorphous Fe_2O_3 and $\text{Ag}_2\text{O}-\text{Fe}_2\text{O}_3$ as Fenton catalysts for degradation of m axilon red dye, *Asia-Pac. J. Chem. Eng.*, 13 (2018) e2184.
- [29] J. Chen, L. Zhang, T. Huang, W. Li, Y. Wang, Z. Wang, Decolorization of azo dye by peroxydisulfate activated by carbon nanotube: radical versus non-radical mechanism, *J. Hazard. Mater.*, 320 (2016) 571–580.
- [30] L. Shen, P. Yan, X. Guo, H. Wei, X. Zheng, Three-dimensional electro-Fenton degradation of methyleneblue based on the composite particle electrodes of carbon nanotubes and nano- Fe_3O_4 , *Arabian J. Sci. Eng.*, 39 (2014) 6659–6664.
- [31] F. Yu, Y. Chen, H. Ma, Ultrahigh yield of hydrogen peroxide and effective diclofenac degradation on a graphite felt cathode loaded with CNTs and carbon black: an electro-generation mechanism and a degradation pathway, *New J. Chem.*, 42 (2018) 4485–4494.
- [32] H. Pourzamani, Y. Hajizadeh, N. Mengelizadeh, Application of three-dimensional electroFenton process using MWCNTs- Fe_3O_4 nanocomposite for removal of diclofenac, *Process Saf. Environ. Prot.*, 119 (2018) 271–284.
- [33] I. Pouladvand, S.K. Asl, M.G. Hoseini, M. Rezvani, Technology, characterization and electrochemical behavior of $\text{Ti}/\text{TiO}_2-\text{RuO}_2-\text{IrO}_2-\text{SnO}_2$ anodes prepared by sol-gel process, *J. Solgel Sci. Technol.*, 89 (2019) 553–561.
- [34] F. Moradi, C. Dehghanian, Addition of IrO_2 to $\text{RuO}_2+\text{TiO}_2$ coated anodes and its effect on electrochemical performance of anodes in acid media, *Prog. Nat. Sci. Mater.*, 24 (2014) 134–141.
- [35] C.-P. Lo, G. Wang, A. Kumar, V. Ramani, $\text{TiO}_2-\text{RuO}_2$ electro-catalyst supports exhibit exceptional electrochemical stability, *Appl. Catal., B*, 140 (2013) 133–140.
- [36] S. Kim, S.K. Choi, B.Y. Yoon, S.K. Lim, H. Park, Effects of electrolyte on the electrocatalytic activities of RuO_2/Ti and $\text{Sb}-\text{SnO}_2/\text{Ti}$ anodes for water treatment, *Appl. Catal., B*, 97 (2010) 135–141.
- [37] T. Saranya, K. Parasuraman, M. Anbarasu, K. Balamurugan, XRD, FT-IR and SEM study of magnetite (Fe_3O_4) nanoparticles prepared by hydrothermal method, *Nano Vision*, 5 (2015) 149–154.
- [38] C. García-Gómez, P. Drogui, F. Zavisca, B. Seyhi, P. Gortáres-Moroyoqui, G. Buelna, C. Neira-Sáenz, M. Estrada-Alvarado, R. Ulloa-Mercado, Experimental design methodology applied to electrochemical oxidation of carbamazepine using Ti/PbO_2 and Ti/BDD electrodes, *J. Electroanal. Chem.*, 732 (2014) 1–10.
- [39] H. Yue, L. Xue, F. Chen, Efficiently electrochemical removal of nitrite contamination with stable $\text{RuO}_2-\text{TiO}_2/\text{Ti}$ electrodes, *Appl. Catal., B*, 206 (2017) 683–691.
- [40] M. Panizza, M.A. Oturan, Degradation of Alizarin Red by electro-Fenton process using a graphite-felt cathode, *Electrochim. Acta*, 56 (2011) 7084–7087.
- [41] H. Mohammadi, B. Bina, A. Ebrahimi, A novel three-dimensional electro-Fenton system and its application for degradation of anti-inflammatory pharmaceuticals: modeling and degradation pathways, *Process Saf. Environ. Prot.*, 117 (2018) 200–213.
- [42] Q. Tang, D. Wang, D. Yao, C. Yang, Y. Sun, Heterogeneous electro-Fenton oxidation of p-nitrophenol with a reusable fluffy clump steel wire, *Desal. Wat. Treat.*, 57 (2016) 15475–15485.
- [43] B. Manu, R. Mahamood, Degradation kinetics of diclofenac in water by Fenton's oxidation, *J. Sustain. Energy Environ.*, 3 (2012) 173–176.
- [44] P. Nidheesh, R. Gandhimathi, S. Velmathi, N. Sanjini, Magnetite as a heterogeneous electro Fenton catalyst for the removal of Rhodamine B from aqueous solution, *RSC Adv.*, 4 (2014) 5698–5708.
- [45] Z. Es' haghzade, E. Pajootan, H. Bahrami, M. Arami, Facile synthesis of Fe_3O_4 nanoparticles via aqueous based electro chemical route for heterogeneous electro-Fenton removal of azo dyes, *J. Taiwan Inst. Chem. Eng.*, 71 (2017) 91–105.
- [46] A. Özcan, A.A. Özcan, Y. Demirci, E. Şener, Preparation of Fe_2O_3 modified kaolin and application in heterogeneous electro-catalytic oxidation of enoxacin, *Appl. Catal., B*, 200 (2017) 361–371.
- [47] H. Pourzamani, H. Mohammadian, N. Niknam, B. Neamati, R. Rahimi, N. Mengelizadeh, Comparison of electrochemical advanced oxidation processes for removal of ciprofloxacin from aqueous solutions, *Desal. Wat. Treat.*, 113 (2018) 307–318.
- [48] A. Shirzadi, A. Nezamzadeh-Ejhi, Enhanced photocatalytic activity of supported $\text{CuO}-\text{ZnO}$ semiconductors towards the photodegradation of mefenamic acid aqueous solution as a semi real sample, *J. Mol. Catal. A-Chem.*, 411 (2016) 222–229.
- [49] X. Wang, K. Zhu, X. Ma, Z. Sun, X. Hu, Degradation of diuron by heterogeneous electro-Fenton using modified magnetic activated carbon as the catalyst, *RSC Adv.*, 8 (2018) 19971–19978.
- [50] C. Zhang, M. Zhou, X. Yu, L. Ma, F. Yu, Modified iron-carbon as heterogeneous electro-Fenton catalyst for organic pollutant degradation in near neutral pH condition: characterization, degradation activity and stability, *Electrochim. Acta*, 160 (2015) 254–262.
- [51] Riyanto, A. Anshori, Electroanalysis of mefenamic acid using platinum powder composite microelectrode (PPCM), *Anal. Bioanal. Chem.*, 6 (2014) 159–169.
- [52] W.N.A.W. Khalit, K.S. Tay, Aqueous chlorination of mefenamic acid: kinetics, transformation by-products and ecotoxicity assessment, *Environ. Sci. Process. Impact.*, 18 (2016) 555–561.